

## Trapping and near-trapping by arrays of cylinders in water waves using the addition theorem and superposition technique

Yi-Jhou Lin<sup>1</sup>, Ying-Te Lee<sup>1</sup> and Jeng-Tzong Chen<sup>1,2\*</sup>

<sup>1</sup> Department of Harbor and River Engineering, National Taiwan Ocean University, Keelung

<sup>2</sup> Department of Mechanical and Mechatronics Engineering, National Taiwan Ocean University, Keelung

No.2, Beining Rd., Jhongjheng District, Keelung City 20224

E-mail: jtchen@mail.ntou.edu.tw

### ABSTRACT

In this paper, we employ the addition theorem and superposition technique to examine the trapped mode of water wave problems. The scattering of water waves by arrays of vertical circular cylinders is solved by using the null-field integral equations in conjunction with degenerate kernels and Fourier series to avoid calculating the Cauchy and Hadamard principal values. In the implementation, the null-field point can be exactly located on the real boundary free of principal-value calculation using bump contour owing to the introduction of degenerate kernels for fundamental solutions. This method can be seen as a semi-analytical approach since errors attribute from the truncation of Fourier series. The physical-resonance phenomena of near-trapped modes are our concern. Several examples are given to demonstrate the validity of the proposed approach.

**KEY WORDS:** Addition theorem; superposition technique; null-field integral equation; Fourier series; trapped mode

### INTRODUCTION

A general problem in offshore engineering is to determine the wave loading exerted upon a circular cylinder. For a single cylinder, an analytical solution was available by MacCamy and Fuchs (1954). For the general case, we always resort to semi-analytical or numerical solutions. A semi-analytical solution using the wave function expansion was obtained by Spring and Monkmeyer (1974) for the diffraction of linear waves by arrays of cylinders. Later, the interaction of water waves with arrays of circular cylinders was studied by Linton and Evans (1990) in a similar way of Twersky approach. Linton and Evans (1990) extended this approach to calculate the force in a more neat form. However, the convergence behavior of the null-field integral equation approach is superior to that of Linton and Evans method. For the boundary integral solution, it converges to  $L_2$  energy sense in an exponential order. It is noted that we can deal with other shape of cross section in our approach, if the degenerate kernels corresponding to the special geometry are available. For example, degenerate kernel for the ellipse can be found in the book of Morse and Feshbach (1978). Also, the work of the elliptic case using the method of Linton and Evans is given in the Martin's book (2006), and the numerical results are implemented by Chatjigeorgiou and Mavrakos (2009). On the other

hand, some formulae are not found in the mathematical handbook or were not derived by mathematicians for the special geometry. That is to say, we have a challenging work in deriving the degenerate kernel for a special geometry case. Besides, our approach can be applied to problems containing both circular and elliptical cylinders since we introduce adaptive coordinate system and vector decomposition. For the Linton and Evans approach, it may have difficulty in their formulation since the addition theorem for translating the polar coordinates to the elliptical coordinates and vice versa is not available to the authors' best knowledge. Simply speaking, the addition theorem is not available to transform Bessel to Mathieu functions when a problem contains circle and ellipse together.

Regarding the numerical methods, Au and Brebbia (1982, 1983) employed the boundary element method (BEM) to calculate the elevation of free surface as well as the resultant force by using constant, linear and quadratic elements. By discretizing the boundary in a more genius way, Zhu and Moule (1996) obtained a more accurate result. Chen (2004) used the composite BEM to determine the free-surface elevation for the porous cylinders. Besides, Chen et al. (2009) employed the null-field integral equation approach to study the near-trapped mode. To determine singular integrals is a critical issue in the boundary integral equation method (BIEM). The present paper is based on the null-field BIEM while the singular integrals are transformed to series sum free of principal-value calculation using bump contour.

Localized oscillations in unbounded media are always referred to trapped modes in different contexts. For example, acoustic resonance, array-guided surface waves, edge waves, Rayleigh-Bloch waves and bound states are similar physical phenomena. Energy in the guided area is stored and can not radiate to infinity in the case of trap wave number. Water wave diffraction and near trapping by a multi-column structure was studied by Evans and Poretr (1997). Near-trapped modes were found for four, five and six cylinders. The wave number to excite the trapped modes was determined numerically by detecting the value of  $ka$  which results in the maximum force. Dirichelet and Neumann trapped modes of large number of cylinders (100) in an infinite domain were found to approach those of infinite number of cylinders by Maniar and Newman (1997). Real and absolute values for the free-surface elevation were investigated by Evans and Porter (1999). Trapped modes for a semi-infinite domain was studied by Thompson et al. (2008). For multiple cylinders in a channel, trapped modes were also found by Evans and Porter (1999). Mathematically speaking, the array-guided cylinders may result in non-trivial solutions of the homogeneous problem at particular values of wave number. It can be understood as eigenvectors corresponding to eigenvalues of certain differential operators on unbounded domains even though there is no characteristic

length as mentioned by Linton and McIver (2007).

Duclos and Cl ement (2004) extended to consider arrays of unevenly spaced cylinders, displaced randomly from a regular array according to a disorder parameter. They focused on two effects of this spacing irregularity, reduction of peak forces associated to trapped mode phenomena, and regularization of the transmission coefficient for waves propagating through the arrays. Also, the reduction of force in the case of near-trapped mode due to disorder is also our interest.

In this paper, the hydrodynamics of circular cylinders is studied by using the null-field integral equation in conjunction with the addition theorem and the Fourier series. The main difference between the present approach and Linton-Evan method is that we use the BIE instead of the wave function expansion. The unknown coefficient here is the Fourier coefficient on the boundary instead of weighting of wave expansion for the domain. The problem can be decomposed into two parts. One is an infinite domain subject to the incident water wave. The other is an exterior Helmholtz problem in an infinite domain with circular boundaries. Force as well as free-surface elevation were calculated and compared with others to check the validity of our formulation. The parameter study for the disorder on the effect of near-trapped modes will be investigated.

## PROBLEM STATEMENT AND INTEGRAL FORMULATION

### Problem statement

Irrotational motion of the inviscid and incompressible fluid is small-amplitude which is defined as velocity potential based on the linear water wave theory. We assume that there are  $N$  vertical circular cylinders mounted at seabed upward to the free surface as shown in Fig. 1. The governing equation of the water wave problem is the Laplace equation

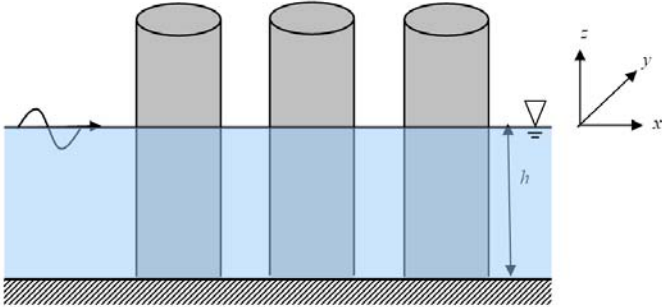


Fig. 1 Problem statement of water waves with an array of vertical cylinders.

$$\nabla^2 \Phi(x, y, z, t) = 0, \quad (x, y, z) \in D. \quad (1)$$

where  $\nabla^2$  and  $D$  are the Laplacian operator and the domain of interest, respectively, and  $\Phi(x, y, z, t)$  is the velocity potential which satisfies the boundary conditions of seabed, kinematic boundary conditions and dynamic boundary condition at free surface as shown below:

$$-\frac{\partial \Phi}{\partial n} = 0, \quad z = -h(x, y), \quad (2)$$

$$-\Phi_z = \varphi_t - \Phi_x \varphi_x - \Phi_y \varphi_y, \quad z = \varphi(x, y, t), \quad (3)$$

$$-\Phi_t + gz + \frac{1}{2}(\Phi_x^2 + \Phi_y^2 + \Phi_z^2), \quad z = \varphi(x, y, t), \quad (4)$$

where  $\varphi(x, y, t)$  is the free-surface elevation. Based on the linear water wave theory and using the technique of separation of separation variable for space and time, we have

$$\Phi(x, y, z, t) = \text{Re}\{u(x, y)f(z)e^{-i\omega t}\}, \quad (5)$$

where

$$f(z) = \frac{-igA}{\omega} \frac{\cosh k(z+h)}{\cosh kh}, \quad (6)$$

in which  $A$  is the amplitude of incident wave,  $g$  is the acceleration of gravity,  $\omega$  denotes the angular frequency,  $k$  represents the wave number, and  $i^2 = -1$ .

where  $\varphi(x, y, t)$  is the free-surface elevation, we assume

$$\varphi(x, y, t) = \text{Re}\{\eta(x, y)e^{-i\omega t}\}, \quad (7)$$

where

$$\eta(x, y) = Au(x, y). \quad (8)$$

The potential of incident wave  $u_{inc}(x, y)$  is shown below:

$$u_{inc}(x, y) = e^{ik(x \cos \theta_{inc} + y \sin \theta_{inc})} \equiv e^{ik\rho \cos(\phi - \theta_{inc})}, \quad (9)$$

where  $\theta_{inc}$  is the angle of incident wave, and  $\rho = \sqrt{x^2 + y^2}$ ,  $\phi = \arctan(y/x)$ . Substituting Eq. (5) into Eq. (1), we have

$$(\nabla^2 + k^2)u(x, y) = 0, \quad (x, y) \in D. \quad (10)$$

Rigid cylinders yield the Neumann boundary conditions as shown below:

$$\frac{\partial u(x, y)}{\partial n} = 0, \quad (x, y) \in B. \quad (11)$$

The dispersion relationship is

$$k \tanh kh = \frac{\omega^2}{g}. \quad (12)$$

The dynamic pressure can be obtained by

$$p = -\rho \frac{\partial \Phi}{\partial t} = -\rho g A \frac{\cosh k(z+h)}{\cosh kh} u(x, y) e^{-i\omega t}, \quad (13)$$

where  $\rho$  is the density of the fluid. The two components of the first-order force  $X^j$  on the  $j$ th cylinder are given by integrating the pressure over the circular boundary as shown below:

$$X^j = -\frac{\rho g A a_j}{k} \tanh kh \int_0^{2\pi} u(x, y) \begin{Bmatrix} \cos \theta_j \\ \sin \theta_j \end{Bmatrix} d\theta_j \quad (14)$$

where  $a_j$  denotes the radius of the  $j$ th cylinder.

### Dual integral equations — the conventional version

The dual boundary integral equation for the domain point can be derived from the Green's third identity (Chen et al., 2003) as given below:

$$2\pi u(\mathbf{x}) = \int_B T(\mathbf{s}, \mathbf{x}) u(\mathbf{s}) dB(\mathbf{s}) - \int_B U(\mathbf{s}, \mathbf{x}) t(\mathbf{s}) dB(\mathbf{s}), \quad \mathbf{x} \in D, \quad (15)$$

$$2\pi t(\mathbf{x}) = \int_B M(\mathbf{s}, \mathbf{x}) u(\mathbf{s}) dB(\mathbf{s}) - \int_B L(\mathbf{s}, \mathbf{x}) t(\mathbf{s}) dB(\mathbf{s}), \quad \mathbf{x} \in D, \quad (16)$$

where  $\mathbf{s}$  and  $\mathbf{x}$  are the source and field points, respectively,

$$t(\mathbf{s}) = \frac{\partial u(\mathbf{s})}{\partial n_s}, \quad B \text{ is the boundary, } n_s \text{ and } n_x \text{ denote the outward normal vectors at the source point } \mathbf{s} \text{ and field point } \mathbf{x}, \text{ respectively.}$$

The kernel function  $U(\mathbf{s}, \mathbf{x})$  is the fundamental solution which satisfies

$$\nabla^2 U(\mathbf{s}, \mathbf{x}) = 2\pi \delta(\mathbf{x} - \mathbf{s}) \quad (17)$$

in which  $\delta(\mathbf{x} - \mathbf{s})$  denotes the Dirac-delta function. Then, we can obtain the fundamental solution as follows

$$U(\mathbf{s}, \mathbf{x}) = \frac{-i\pi H_0^{(1)}(kr)}{2} \quad (18)$$

where  $H_0^{(1)}(kr)$  is the zeroth Hankel function of the first kind and  $r \equiv |\mathbf{s} - \mathbf{x}|$ . The other kernels functions,  $T(\mathbf{s}, \mathbf{x})$ ,  $L(\mathbf{s}, \mathbf{x})$ , and  $M(\mathbf{s}, \mathbf{x})$ , are defined by

$$T(\mathbf{s}, \mathbf{x}) = \frac{\partial U(\mathbf{s}, \mathbf{x})}{\partial n_s}, \quad (19)$$

$$L(\mathbf{s}, \mathbf{x}) = \frac{\partial U(\mathbf{s}, \mathbf{x})}{\partial n_x}, \quad (20)$$

$$M(\mathbf{s}, \mathbf{x}) = \frac{\partial^2 U(\mathbf{s}, \mathbf{x})}{\partial n_s \partial n_x}. \quad (21)$$

By moving the field point  $x$  to the boundary, the dual boundary integral equations for the boundary point can be obtained as follows:

$$\pi u(\mathbf{x}) = C.P.V. \int_B T(\mathbf{s}, \mathbf{x}) u(\mathbf{s}) dB(\mathbf{s}) - R.P.V. \int_B U(\mathbf{s}, \mathbf{x}) t(\mathbf{s}) dB(\mathbf{s}), \quad x \in B, \quad (22)$$

$$\pi t(\mathbf{x}) = H.P.V. \int_B M(\mathbf{s}, \mathbf{x}) u(\mathbf{s}) dB(\mathbf{s}) - C.P.V. \int_B L(\mathbf{s}, \mathbf{x}) t(\mathbf{s}) dB(\mathbf{s}), \quad x \in B, \quad (23)$$

where  $R.P.V.$ ,  $C.P.V.$  and  $H.P.V.$  denote the Riemann, Cauchy and Hadamard (or called Mangler) principal values, respectively. By moving the field point to the complementary domain, the dual null-field integral equations are given below

$$0 = \int_B T(\mathbf{s}, \mathbf{x}) u(\mathbf{s}) dB(\mathbf{s}) - \int_B U(\mathbf{s}, \mathbf{x}) t(\mathbf{s}) dB(\mathbf{s}), \quad x \in D^c, \quad (24)$$

$$0 = \int_B M(\mathbf{s}, \mathbf{x}) u(\mathbf{s}) dB(\mathbf{s}) - \int_B L(\mathbf{s}, \mathbf{x}) t(\mathbf{s}) dB(\mathbf{s}), \quad x \in D^c, \quad (25)$$

where  $D^c$  is the complementary domain. Eqs. (15), (16), (24) and (25) are conventional formulations where the point can not be located on the real boundary. Singularity occurs and concept of principal values is required once Eqs. (22) and (23) are considered.

### Dual boundary integral formulation — the present version

By introducing the degenerate kernel, the collocation point can be exactly located on the real boundary free of calculating singular integrals in the sense of principal value. Therefore, the integral equations for the domain point and null-field integral equations in the interior problem are represented as

$$2\pi u(x) = \int_B T^I(\mathbf{s}, \mathbf{x}) u(\mathbf{s}) dB(\mathbf{s}) - \int_B U^I(\mathbf{s}, \mathbf{x}) t(\mathbf{s}) dB(\mathbf{s}), \quad x \in D \cup B, \quad (26)$$

$$2\pi t(\mathbf{x}) = \int_B M^I(\mathbf{s}, \mathbf{x}) u(\mathbf{s}) dB(\mathbf{s}) - \int_B L^I(\mathbf{s}, \mathbf{x}) t(\mathbf{s}) dB(\mathbf{s}), \quad x \in D \cup B, \quad (27)$$

and

$$0 = \int_B T^E(\mathbf{s}, \mathbf{x}) u(\mathbf{s}) dB(\mathbf{s}) - \int_B U^E(\mathbf{s}, \mathbf{x}) t(\mathbf{s}) dB(\mathbf{s}), \quad x \in D^c \cup B, \quad (28)$$

$$0 = \int_B M^E(\mathbf{s}, \mathbf{x}) u(\mathbf{s}) dB(\mathbf{s}) - \int_B L^E(\mathbf{s}, \mathbf{x}) t(\mathbf{s}) dB(\mathbf{s}), \quad x \in D^c \cup B. \quad (29)$$

For the exterior problem, the domain of interest is in the external region of the circular boundary and the complementary domain is in the internal region of the circle. Therefore, the null-field integral equations are represented as

$$2\pi u(x) = \int_B T^E(\mathbf{s}, \mathbf{x}) u(\mathbf{s}) dB(\mathbf{s}) - \int_B U^E(\mathbf{s}, \mathbf{x}) t(\mathbf{s}) dB(\mathbf{s}), \quad x \in D \cup B, \quad (23)$$

$$2\pi t(\mathbf{x}) = \int_B M^E(\mathbf{s}, \mathbf{x}) u(\mathbf{s}) dB(\mathbf{s}) - \int_B L^E(\mathbf{s}, \mathbf{x}) t(\mathbf{s}) dB(\mathbf{s}), \quad x \in D \cup B, \quad (31)$$

and

$$0 = \int_B T^I(\mathbf{s}, \mathbf{x}) u(\mathbf{s}) dB(\mathbf{s}) - \int_B U^I(\mathbf{s}, \mathbf{x}) t(\mathbf{s}) dB(\mathbf{s}), \quad x \in D^c \cup B, \quad (32)$$

$$0 = \int_B M^I(\mathbf{s}, \mathbf{x}) u(\mathbf{s}) dB(\mathbf{s}) - \int_B L^I(\mathbf{s}, \mathbf{x}) t(\mathbf{s}) dB(\mathbf{s}), \quad x \in D^c \cup B, \quad (33)$$

where the superscripts of “ $I$ ” and “ $E$ ” denote interior and exterior degenerate kernels for fundamental solutions. The explicit forms of degenerate kernels will be elaborated on later.

### Expansions of fundamental solution and boundary density

Based on the separable property, the kernel function  $U(\mathbf{s}, \mathbf{x})$  can be expanded into degenerate form by separating the source point and field point in the polar coordinates. Since degenerate kernels can describe the fundamental solutions in two regions (interior and exterior domains), the BIE for the domain point in Eqs. (26)-(27) and Eqs. (30)-(31) and the null-field BIE in Eqs. (28)-(29) and Eqs. (32)-(33), can be directly employed for the real boundary point. By using the polar

coordinates, we can express  $\mathbf{x} = (\rho, \phi)$  and  $\mathbf{s} = (R, \theta)$ . The four kernels  $U$ ,  $T$ ,  $L$  and  $M$  can be expressed in terms of degenerate kernels (Chen *et al.*, 2007) as shown below:

$$U(\mathbf{s}, \mathbf{x}) = \begin{cases} U^I(R, \theta; \rho, \phi) = \frac{-\pi i}{2} \sum_{m=0}^{\infty} \varepsilon_m J_m(k\rho) H_m^{(1)}(kR) \\ \quad \cos(m(\theta - \phi)), \quad R \geq \rho, \\ U^E(R, \theta; \rho, \phi) = \frac{-\pi i}{2} \sum_{m=0}^{\infty} \varepsilon_m H_m^{(1)}(k\rho) J_m(kR) \\ \quad \cos(m(\theta - \phi)), \quad R < \rho, \end{cases} \quad (34)$$

$$T(\mathbf{s}, \mathbf{x}) = \begin{cases} T^I(R, \theta; \rho, \phi) = \frac{-\pi k i}{2} \sum_{m=0}^{\infty} \varepsilon_m J_m(k\rho) H_m^{(1)}(kR) \\ \quad \cos(m(\theta - \phi)), \quad R > \rho, \\ T^E(R, \theta; \rho, \phi) = \frac{-\pi k i}{2} \sum_{m=0}^{\infty} \varepsilon_m H_m^{(1)}(k\rho) J_m'(kR) \\ \quad \cos(m(\theta - \phi)), \quad R < \rho, \end{cases} \quad (35)$$

$$L(\mathbf{s}, \mathbf{x}) = \begin{cases} L^I(R, \theta; \rho, \phi) = \frac{-\pi k i}{2} \sum_{m=0}^{\infty} \varepsilon_m J_m'(k\rho) H_m^{(1)}(kR) \\ \quad \cos(m(\theta - \phi)), \quad R > \rho, \\ L^E(R, \theta; \rho, \phi) = \frac{-\pi k i}{2} \sum_{m=0}^{\infty} \varepsilon_m H_m^{(1)}(k\rho) J_m(kR) \\ \quad \cos(m(\theta - \phi)), \quad R < \rho, \end{cases} \quad (36)$$

$$M(\mathbf{s}, \mathbf{x}) = \begin{cases} M^I(R, \theta; \rho, \phi) = \frac{-\pi k^2 i}{2} \sum_{m=0}^{\infty} \varepsilon_m J_m(k\rho) H_m^{(1)}(kR) \\ \quad \cos(m(\theta - \phi)), \quad R \geq \rho, \\ M^E(R, \theta; \rho, \phi) = \frac{-\pi k^2 i}{2} \sum_{m=0}^{\infty} \varepsilon_m H_m^{(1)}(k\rho) J_m'(kR) \\ \quad \cos(m(\theta - \phi)), \quad R < \rho, \end{cases} \quad (37)$$

where  $\varepsilon_m$  is the Neumann factor

$$\varepsilon_m = \begin{cases} 1, & m = 0, \\ 2, & m = 1, 2, \dots, \infty. \end{cases} \quad (38)$$

Mathematically speaking, the expressions of fundamental solutions in Eqs. (34)-(37) are termed degenerate kernels (or separable kernels) which can expand the kernel to sums of products of function of the field point  $x$  alone and functions of the source point  $s$  alone. If the finite sum of series is considered, the kernel is finite rank. As we shall see in the later sections, the theory of boundary integral equations with degenerate kernel is nothing more than the linear algebra. Since the potentials resulted from  $T(s, x)$  and  $L(s, x)$  are discontinuous across the boundary, the potentials of  $T(s, x)$  and  $L(s, x)$  for  $R \rightarrow \rho^+$  and  $R \rightarrow \rho^-$  are different. This is the reason why the equal sign between  $\rho$  and  $R$  is not included in the expression for the degenerate kernels of  $T(s, x)$  and  $L(s, x)$  in Eqs. (35) and (36). The degenerate kernels simply serve as the means to evaluate regular integrals analytically and take the limit to boundary analytically. The reason is that integral equation for the domain point of Eq. (27) and the null-field integral equation of Eq. (29) yield the same linear algebraic equation when the limit is taken from the inside or from the outside of the region. Both limits represent the same algebraic equation that is an approximate counterpart of the boundary integral equation, that for the case of a smooth boundary has in the left-hand side term  $\pi u(\mathbf{x})$  or  $\pi t(\mathbf{x})$  rather than  $2\pi u(\mathbf{x})$  or  $2\pi t(\mathbf{x})$  for the domain point or 0 for the point outside the domain. Besides, the limiting case to the boundary is also addressed. The continuous and jump behavior across the boundary is well captured by the Wronskian property of Bessel function  $J_m$  and  $Y_m$  bases

$$W(J_m(kR), Y_m(kR)) = Y_m'(kR) J_m(kR) - Y_m(kR) J_m'(kR) = \frac{2}{\pi k R} \quad (39)$$

as shown below

$$\int_0^{2\pi} (T^I(\mathbf{s}, \mathbf{x}) - T^E(\mathbf{s}, \mathbf{x})) \cos(m\theta) R d\theta = 2\pi \cos(m\phi), \quad x \in B, \quad (40)$$

$$\int_0^{2\pi} (T^I(\mathbf{s}, \mathbf{x}) - T^E(\mathbf{s}, \mathbf{x})) \sin(m\theta) R d\theta = 2\pi \sin(m\phi), \quad x \in B. \quad (41)$$

After employing Eqs. (40)-(41), Eq.(30) and Eq. (32) yield the same linear algebraic equation when  $x$  is exactly located the boundary from the domain or the complementary domain. A proof for the Laplace case can be found by Chen *et al.* (2006).

In order to fully utilize the geometry of circular boundary, the boundary potential  $u(\mathbf{s})$  and its normal flux  $t(\mathbf{s})$  can be approximated by employing the Fourier series. Therefore, we obtain

$$u(\mathbf{s}) = a_0 + \sum_{n=1}^{\infty} (a_n \cos n\theta + b_n \sin n\theta), \quad (42)$$

$$t(\mathbf{s}) = p_0 + \sum_{n=1}^{\infty} (p_n \cos n\theta + q_n \sin n\theta), \quad (43)$$

where  $a_0$ ,  $a_n$ ,  $b_n$ ,  $p_0$ ,  $p_n$  and  $q_n$  are the Fourier coefficients. Eqs. (32) and (33) can be easily calculated by employing the orthogonal property of Fourier series. In the real computation, only the finite  $M$  terms are used in the summation of Eqs. (42) and (43).

### Adaptive observer system

Since the boundary integral equations are frame indifferent, *i.e.* rule of objectivity is obeyed. Adaptive observer system is chosen to fully employ the property of degenerate kernels. Fig. 2 shows the boundary integration for the circular boundaries. It is worthy of noting that the origin of the observer system can be adaptively located on the center of the corresponding circle under integration to fully utilize the geometry of circular boundary. The dummy variable in the integration on the circular boundary is just the angle ( $\theta$ ) instead of the radial coordinate ( $R$ ). By using the adaptive observer system, all the boundary integrals can be determined analytically free of principal-value calculation using bump contour.

### Linear Algebraic Equation

After locating the null-field point  $x_k$  exactly on the  $k$ th circular boundary in Eq. (28) as shown in Fig. 2, we have

$$0 = \sum_{k=0}^N \int_{B_k} T^E(\mathbf{s}, \mathbf{x}) u(\mathbf{s}) dB(\mathbf{s}) - \sum_{k=0}^N \int_{B_k} U^E(\mathbf{s}, \mathbf{x}) t(\mathbf{s}) dB(\mathbf{s}), \quad x \in D^c \cup B, \quad (44)$$

where  $N$  is the number of circular cylinders and  $B_0$  denotes the outer boundary for the bounded domain. In case of the infinite problem,  $B_0$  becomes  $B_{\infty}$ . The origin of observer system is adaptively chosen at the center of circular boundary under integration. The dummy variable in the circular integration is angle ( $\theta$ ) instead of radial coordinate ( $R$ ). In the real computation, we select the collocation point on the boundary and the integration path is counterclockwise for the outer circle. Otherwise, it is clockwise. For the integration path  $B_k$ , the kernels of  $U(\mathbf{s}, \mathbf{x})$  and  $T(\mathbf{s}, \mathbf{x})$  are respectively expressed in terms of degenerate kernels of Eqs. (33) and (34) with respect to the observer origin at the center of the corresponding path. The boundary densities of  $u(\mathbf{s})$  and  $t(\mathbf{s})$  are substituted by using the Fourier series of Eqs. (42) and (43), respectively. In the  $B_k$  integration, we set the origin of the observer system to collocate at the center  $c_k$  of  $B_k$  to fully utilize the degenerate kernel and Fourier series. By moving the null-field point exactly on the real boundary  $B_k$  from outside of the domain  $D^c$  in the numerical implementation, a linear algebraic system is obtained.

$$[\mathbf{U}]\{\mathbf{t}\} = [\mathbf{T}]\{\mathbf{u}\}, \quad (45)$$

where  $[\mathbf{U}]$  and  $[\mathbf{T}]$  are the influence matrices with a dimension of  $N \times (2M+1)$  by  $N \times (2M+1)$ ,  $\{\mathbf{t}\}$  and  $\{\mathbf{u}\}$  denote the vectors for  $t(\mathbf{s})$  and  $u(\mathbf{s})$  of the Fourier coefficients with a dimension of  $N \times (2M+1)$  by 1, in which,  $[\mathbf{U}]$ ,  $[\mathbf{T}]$ ,  $\{\mathbf{u}\}$  and  $\{\mathbf{t}\}$  are defined as follows:

$$[\mathbf{U}] = \begin{bmatrix} \mathbf{U}_{11} & \mathbf{U}_{12} & \cdots & \mathbf{U}_{1N} \\ \mathbf{U}_{21} & \mathbf{U}_{22} & \cdots & \mathbf{U}_{2N} \\ \vdots & \vdots & \ddots & \vdots \\ \mathbf{U}_{N1} & \mathbf{U}_{N2} & \cdots & \mathbf{U}_{NN} \end{bmatrix} \quad (46)$$

$$[\mathbf{T}] = \begin{bmatrix} \mathbf{T}_{11} & \mathbf{T}_{12} & \cdots & \mathbf{T}_{1N} \\ \mathbf{T}_{21} & \mathbf{T}_{22} & \cdots & \mathbf{T}_{2N} \\ \vdots & \vdots & \ddots & \vdots \\ \mathbf{T}_{N1} & \mathbf{T}_{N2} & \cdots & \mathbf{T}_{NN} \end{bmatrix}, \quad (47)$$

$$\{\mathbf{u}\} = \begin{Bmatrix} \mathbf{u}_1 \\ \mathbf{u}_2 \\ \vdots \\ \mathbf{u}_N \end{Bmatrix}, \quad \{\mathbf{t}\} = \begin{Bmatrix} \mathbf{t}_1 \\ \mathbf{t}_2 \\ \vdots \\ \mathbf{t}_N \end{Bmatrix} \quad (48)$$

where the vectors  $\{\mathbf{u}_k\}$  and  $\{\mathbf{t}_k\}$  are in the form of  $\{a_0^k \ a_1^k \ b_1^k \ \cdots \ a_M^k \ b_M^k\}^T$  and  $\{p_0^k \ p_1^k \ q_1^k \ \cdots \ p_M^k \ q_M^k\}^T$ ; the first subscript “ $j$ ” ( $j=1, 2, \dots, N$ ) in the  $[\mathbf{U}_{jk}]$  denotes the index of the  $j$ th circle where the collocation point is located and the second subscript “ $k$ ” ( $k=1, 2, \dots, N$ ) denotes the index of the  $k$ th circle where the boundary data  $\{\mathbf{u}_k\}$  or  $\{\mathbf{t}_k\}$  are routed. The number of circular holes is  $N$  and the highest harmonic of truncated terms is  $M$ . The coefficient matrix of the linear algebraic system is partitioned into blocks, and each diagonal block ( $\mathbf{U}_{mm}$ ) corresponds to the influence matrices due to the same circle of collocation and Fourier expansion. After uniformly collocating the point along the  $j$ th circular boundary, the sub-matrix can be written as

$$[\mathbf{U}_{jk}] = \begin{bmatrix} \mathbf{U}_{jk}^{0c}(\phi_1) & \mathbf{U}_{jk}^{1c}(\phi_1) & \mathbf{U}_{jk}^{2s}(\phi_1) \\ \mathbf{U}_{jk}^{0c}(\phi_2) & \mathbf{U}_{jk}^{1c}(\phi_2) & \mathbf{U}_{jk}^{2s}(\phi_2) \\ \mathbf{U}_{jk}^{0c}(\phi_3) & \mathbf{U}_{jk}^{1c}(\phi_3) & \mathbf{U}_{jk}^{2s}(\phi_3) \\ \vdots & \vdots & \vdots \\ \mathbf{U}_{jk}^{0c}(\phi_{2M}) & \mathbf{U}_{jk}^{1c}(\phi_{2M}) & \mathbf{U}_{jk}^{2s}(\phi_{2M}) \\ \mathbf{U}_{jk}^{0c}(\phi_{2M+1}) & \mathbf{U}_{jk}^{1c}(\phi_{2M+1}) & \mathbf{U}_{jk}^{2s}(\phi_{2M+1}) \\ \cdots & \mathbf{U}_{jk}^{Mc}(\phi_1) & \mathbf{U}_{jk}^{Ms}(\phi_1) \\ \cdots & \mathbf{U}_{jk}^{Mc}(\phi_2) & \mathbf{U}_{jk}^{Ms}(\phi_2) \\ \cdots & \mathbf{U}_{jk}^{Mc}(\phi_3) & \mathbf{U}_{jk}^{Ms}(\phi_3) \\ \vdots & \vdots & \vdots \\ \cdots & \mathbf{U}_{jk}^{Mc}(\phi_{2M}) & \mathbf{U}_{jk}^{Ms}(\phi_{2M}) \\ \cdots & \mathbf{U}_{jk}^{Mc}(\phi_{2M+1}) & \mathbf{U}_{jk}^{Ms}(\phi_{2M+1}) \end{bmatrix} \quad (49)$$

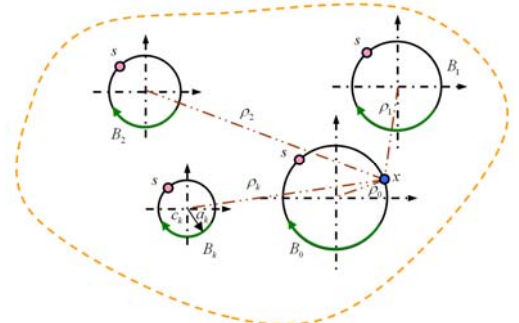


Fig. 2 An adaptive observer system.

$$[\mathbf{T}_{jk}] = \begin{bmatrix} \mathbf{T}_{jk}^{0c}(\phi_1) & \mathbf{T}_{jk}^{1c}(\phi_1) & \mathbf{T}_{jk}^{2s}(\phi_1) \\ \mathbf{T}_{jk}^{0c}(\phi_2) & \mathbf{T}_{jk}^{1c}(\phi_2) & \mathbf{T}_{jk}^{2s}(\phi_2) \\ \mathbf{T}_{jk}^{0c}(\phi_3) & \mathbf{T}_{jk}^{1c}(\phi_3) & \mathbf{T}_{jk}^{2s}(\phi_3) \\ \vdots & \vdots & \vdots \\ \mathbf{T}_{jk}^{0c}(\phi_{2M}) & \mathbf{T}_{jk}^{1c}(\phi_{2M}) & \mathbf{T}_{jk}^{2s}(\phi_{2M}) \\ \mathbf{T}_{jk}^{0c}(\phi_{2M+1}) & \mathbf{T}_{jk}^{1c}(\phi_{2M+1}) & \mathbf{T}_{jk}^{2s}(\phi_{2M+1}) \\ \dots & \mathbf{T}_{jk}^{Mc}(\phi_1) & \mathbf{T}_{jk}^{Ms}(\phi_1) \\ \dots & \mathbf{T}_{jk}^{Mc}(\phi_2) & \mathbf{T}_{jk}^{Ms}(\phi_2) \\ \dots & \mathbf{T}_{jk}^{Mc}(\phi_3) & \mathbf{T}_{jk}^{Ms}(\phi_3) \\ \vdots & \vdots & \vdots \\ \dots & \mathbf{T}_{jk}^{Mc}(\phi_{2M}) & \mathbf{T}_{jk}^{Ms}(\phi_{2M}) \\ \dots & \mathbf{T}_{jk}^{Mc}(\phi_{2M+1}) & \mathbf{T}_{jk}^{Ms}(\phi_{2M+1}) \end{bmatrix} \quad (50)$$

It is noted that the superscript "0s" in Eq. (49) disappears since  $\sin(0\theta) = 0$ , and the element of  $[\mathbf{U}_{jk}]$  and  $[\mathbf{T}_{jk}]$  are defined as

$$U_{jk}^{nc} = \int_{B_k} U(s_k, x_m) \cos(n\theta_k) R_k d\theta_k \quad (51)$$

$$U_{jk}^{ns} = \int_{B_k} U(s_k, x_m) \sin(n\theta_k) R_k d\theta_k \quad (52)$$

$$T_{jk}^{nc} = \int_{B_k} T(s_k, x_m) \cos(n\theta_k) R_k d\theta_k \quad (53)$$

$$T_{jk}^{ns} = \int_{B_k} T(s_k, x_m) \sin(n\theta_k) R_k d\theta_k \quad (54)$$

where  $n = 1, 2, \dots, M$ . After obtaining the unknown Fourier coefficients, the origin of observer system is set to  $c_j$  in the  $B_j$  integration as shown in Fig. 3 to obtain the interior potential by employing Eq.(26) and (30).

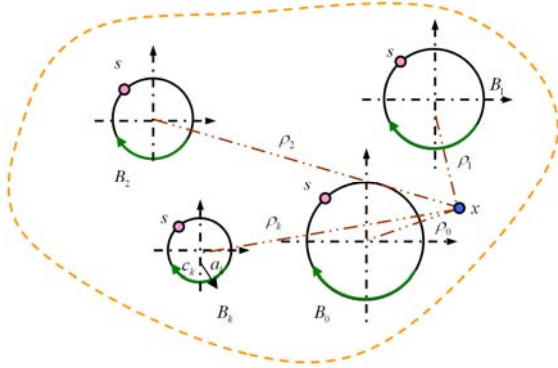


Fig. 3 Sketch of the BIE for the domain point.

### Perturbation of ordered cylinder arrangements

An array of cylinders according to a regular three-rows disposition is shown in Fig. 4. For the purpose of disturbing the regular arrangement, a perturbation of disposition is given. The displacement of each cylinder center apart from its original periodical position is defined as follows

$$\begin{aligned} \Delta x_j &= \gamma_j p \tau \cos(2\pi\gamma_j), \\ \Delta y_j &= \gamma_j p \tau \sin(2\pi\gamma_j), \end{aligned} \quad (55)$$

where  $\gamma_j$  is a random variable in the range of  $[0,1]$ , the maximum permissible displacement  $p$  is equal to  $d-a$  and  $\tau$  is a global disorder parameter. The distance between the two centers of identical cylinders is  $2d$  where the radii of cylinders are  $a$ .

### Illustrative examples

In this paper, we concern with the effect of disorder ( $\tau$ ) on the near-trapped modes. Several examples including four, six, ten and sixteen cylinders as shown in Fig. 4 are given to verify the validity of our approach.

Case 1: four cylinders

Figs. 5 (a) and (b) give the original state for the trapped mode without disturbance due to disorder ( $\tau = 0$ ) in the case of wave number  $k = 4.08482$  by using Evans and Porter's approach and our approach, respectively. Both figures show the contour of absolute value of free-surface elevation for  $a/d = 0.8$ . As predicted by Evans and Porter (1999), we reconfirm that over 150 times of the amplitude of incident wave and 54 times of the force over one isolated cylinder using our approach.

Case 2: six cylinders

For one set of six cylinders as shown in Fig. 4(b), Figs. 6 (a) and (b) also show the contour plots of trapped modes by using Evan and Porter's approach and our method, respectively.

Case 3: ten cylinders

For the array of three sets, ten cylinders is considered. The absolute value of potential is plotted and the near-trapped mode is also observed by using our approach in Fig. 7.

Case 4: sixteen cylinders

For the five sets of sixteen cylinders, contour plots of the maximum free-surface elevation are shown in Figs. 8 (a) and (b) by using the Duclos and Clément's method (2004) and our approach, respectively. The maximum wave amplitude is predicted to be about 150 times by using both approaches. We also show the 3-D plot of our result in Fig. 8 (c). Figs. 9 (a) and (b) show the force experienced by cylinder No.3 of the linear array in Fig. 4(d) and cylinder 1 (see Fig. 4(a)) of the circular cylinders by using the Duclos and Clément's method (2004) and our approach, respectively. Agreement is observed for the maximum resultant force. For this critical wave number, we find a very large and sharp peak up to 46 times the force on a single identical cylinder in the same field.

Following the definition of disorder parameter  $\tau$ , two random cases of  $\tau = 0.1$  were reported by Duclos and Clément (2004) as shown in Figs. 10 (a) and (b). The appearance of the trapped mode is dramatically suppressed. To test the accuracy of our approach for the disorder effect, Fig. 11 shows that the contour plot of the trapped mode is effectively suppressed for  $\tau = 0.1$ .

### CONCLUSIONS

In this paper, not only a systematic approach was employed to investigate the water-wave interaction with arrays of cylinders, but also the effect of disorder on the force in case of trapped modes was also examined. Addition theorem or so-called the degenerate kernel is adopted in the null-field integral formulation. Therefore, the singular integrals using bump integrals for principal values can be avoided. Numerical results including the free-surface elevation and resultant forces on each cylinder have been presented to illustrate the effect of disorder parameter on the force in case of trapped modes. Good agreements are observed after comparing with the results obtained in the literature.

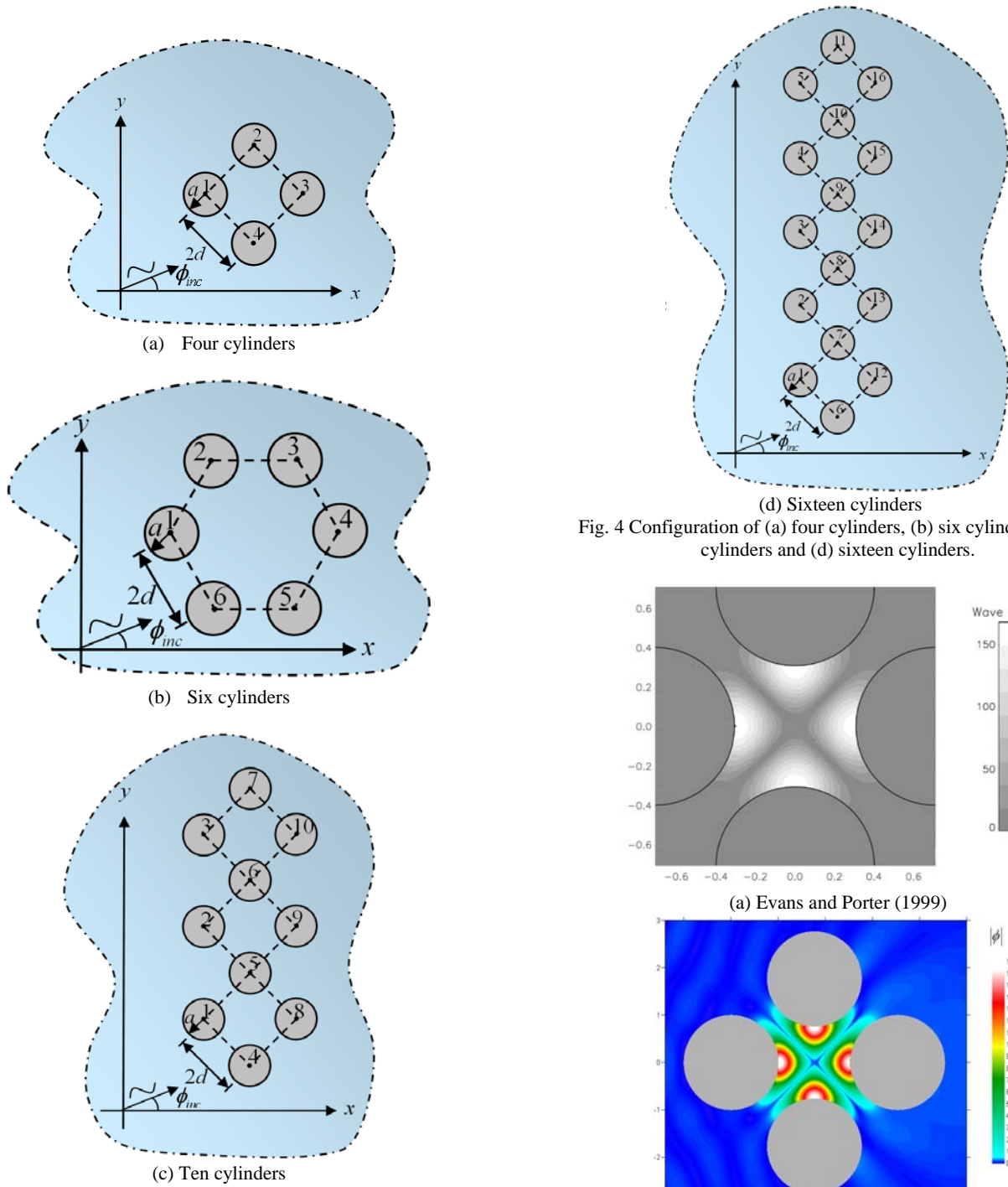


Fig. 4 Configuration of (a) four cylinders, (b) six cylinders, (c) ten cylinders and (d) sixteen cylinders.

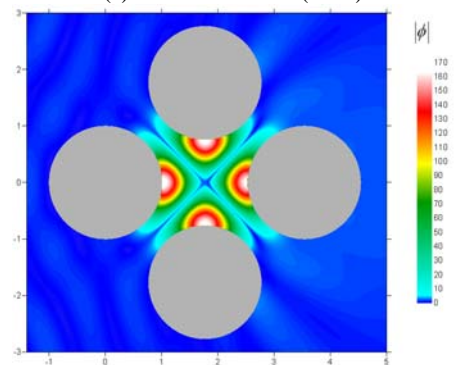
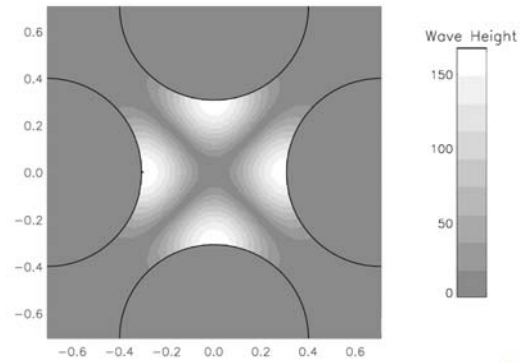
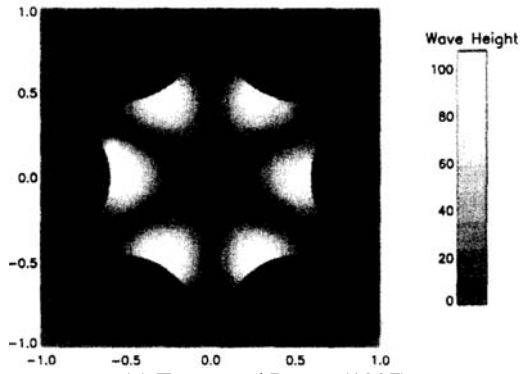
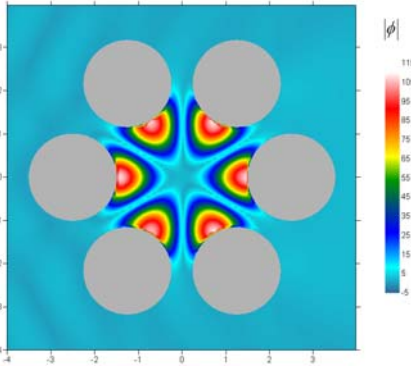


Fig. 5 Near-trapped mode for the four cylinders at  $ka=4.08482$  ( $a/d=0.8$ ,  $\tau=0.0$ )

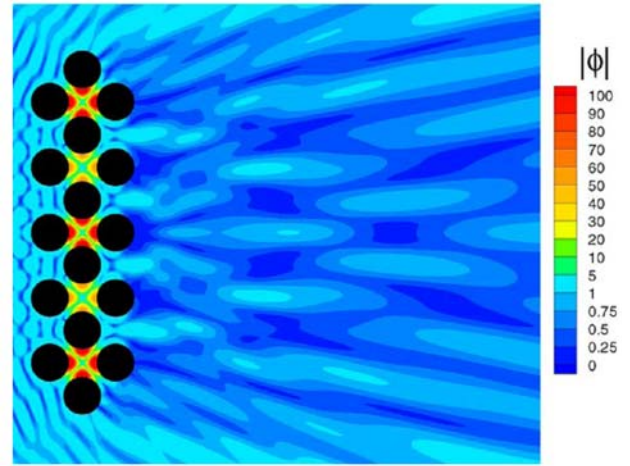


(a) Evans and Porter (1997)

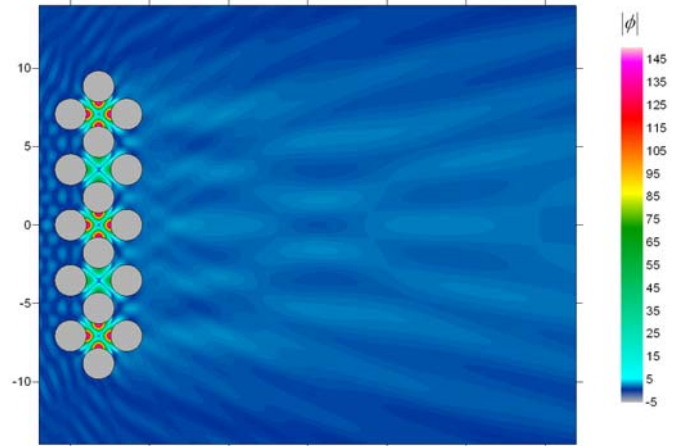


(b) Present method ( $M=20$ )

Fig. 6 Near-trapped mode for the six cylinders at  $ka=2.92921$  ( $a/d=0.8$ ,  $\tau=0.0$ )



(a) Contour plot by Duclos and Clément (2004)



(b) Contour plot by using the present method ( $M=20$ )

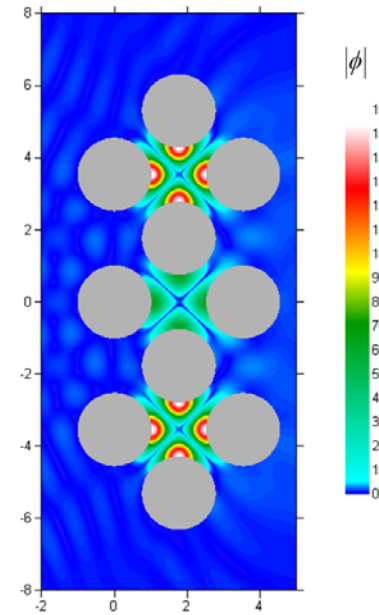
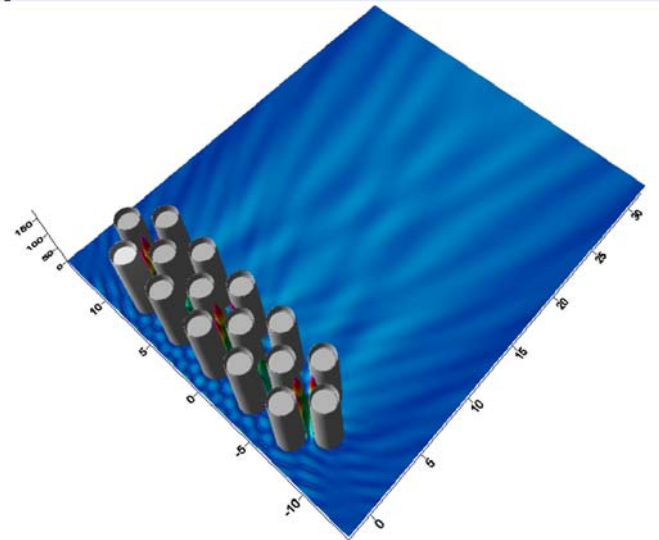


Fig. 7 Near-trapped mode for the ordered pile array at  $ka=4.08482$  ( $a/d=0.8$ ,  $M=20$ ,  $\tau=0.0$ )



(c) Free-surface elevations by the present method ( $M=20$ )  
 Fig. 8 Near-trapped mode for the ordered pile array at  $ka=4.08482$  ( $a/d=0.8$ ,  $M=20$ ,  $\tau=0.0$ )

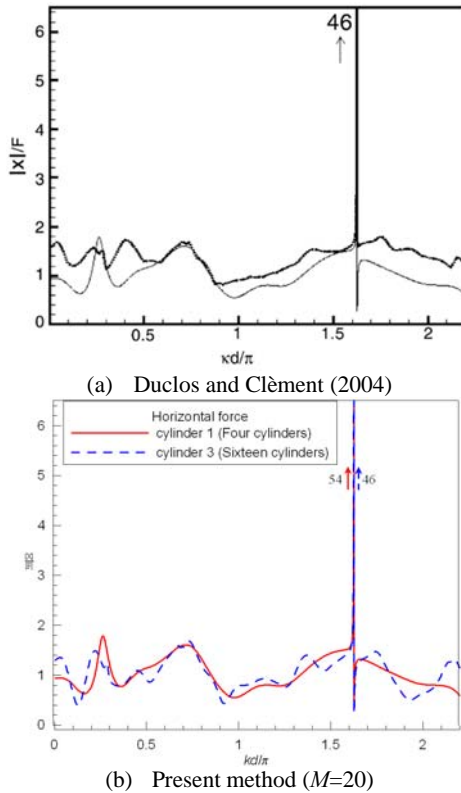


Fig. 9 Horizontal force on the corresponding cylinder of the ordered pile array. ( $kd/\pi=1.625293$ ,  $a/d=0.8$ ,  $M=20$ ,  $\tau=0.0$ )

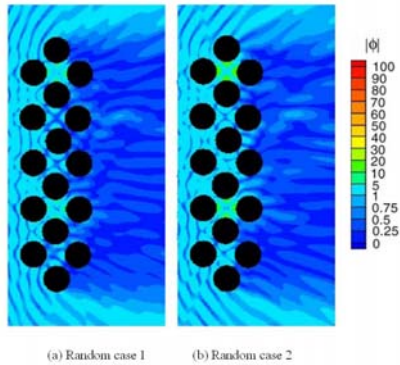


Fig. 10 Suppression of near-trapped modes by using disorder ( $\tau=0.1$ , Duclos and Clément, 2004).

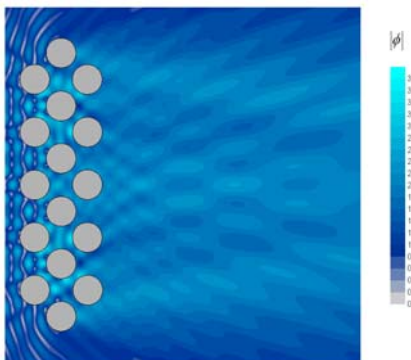


Fig. 11 Suppression of near-trapped modes by using disorder. ( $a/d=0.8$ ,  $M=20$ )

## REFERENCES

- Au, MC, and Brebbia, CA (1982). "Numerical prediction of wave forces using the boundary element method," *Appl Math Model*, Vol 6, pp 218-228.
- Au, MC, and Brebbia, CA (1983). "Diffraction of water waves for vertical cylinders using boundary elements," *Appl Math Model*, Vol 7, pp 106-114.
- Chen, JT, Chen, KH, Chen, IL and Liu, LW (2003). "A new concept of modal participation factor for numerical instability in the dual BEM for exterior acoustics." *Mech Res Commun*, Vol 26, No 2, pp 161-174.
- Chen, JT, Shen, WC, and Wu, AC (2006). "Null-field integral equations for stress field around circular holes under antiplane shear." *Eng Anal Bound Elem*, Vol 30, pp 205-217.
- Chen, JT, Chen, CT, Chen, PY and Chen, IL (2007). "A semi-analytical approach for radiation and scattering." *Comput Methods Appl Mech Engrg*, Vol 196, pp 2751-2764.
- Chen, YH (2004). "Wave-induced oscillations in harbors by permeable arc breakwaters," *Master Thesis*, National Taiwan Ocean University, Keelung.
- Chen, JT, Lee, YT and Lin, YJ (2009). "Interaction of water waves with arbitrary vertical cylinders using null-field integral equations." *Appl Ocean Res*, Accepted.
- Chatjigeorgiou, IK, Mavrakos, SA (2009). "Hydrodynamic diffraction by multiple elliptical cylinders." The 24th International Workshop on Water Waves and Floating Bodies. Zelenogorsk, Russia.
- Duclos, G, and Clément, AH (2004). "Wave propagation through arrays of unevenly spaced vertical piles," *Ocean Eng*, Vol 31, pp 1655-1668.
- Evans, DV, and Porter, R (1997). "Trapped modes about multiple cylinders in a channel," *J Fluid Mech*, Vol 339, pp 331-356.
- Evans, DV, and Porter, R. (1999). "Trapping and near-trapping by arrays of cylinders in waves," *J Fluid Mech*, Vol 35, pp 149-179.
- Linton, CM, and Evans, DV (1990). "The interaction of waves with arrays of vertical circular cylinders," *J Fluid Mech*, Vol 215, pp 549-569.
- Linton, CM, and McIver, P (2007). "Embedded trapped modes in water waves and acoustics." *Wave Motion*, Vol 45, pp 16-29.
- Maniar, HD, and Newman, JN (1997). "Wave diffraction by a long array of cylinders," *J Fluid Mech*, Vol 339, pp309-330.
- Morse, PM, Feshbach, H (1978). "Methods of theoretical physics." New York: McGraw-Hill.
- Martin, PA (2006). "Multiple Scattering. Interaction of time-harmonic waves with N obstacles." New York: Cambridge University Press.
- MacCamy, RC, and Fuchs, RA (1954). "Wave force on piles: A diffraction theory." *Technical Memorandum No. 69 U. S. Army Coastal Engineering Research Center (formerly Beach Erosion Board)*.
- Spring, BH, and Monkmeyer, PL (1974). "Interaction of plane waves with vertical cylinders," *Proceeding 14th International Conference on Coastal Engineering*, pp 1828-1845.
- Thompson, I, Linton, CM, and Porter, R (2008). "A new approximation method for scattering by long finite arrays," *Q J Mech Appl Math*, Vol 25, pp 333-352.
- Williams, AN, and Li, W (2000). "Water wave interaction with an array of bottom-mounted surface-piercing porous cylinders." *Ocean Eng*, Vol 27, pp 841-866.
- Zhu, SP, and Moule, G (1996). "An Efficient Numerical Calculation of Wave Loads on an Array of Vertical Cylinders." *Appl Math Model*, Vol 20, pp 26-33.